Surface-Impedance Boundary Conditions in Dual Time-Domain Finite-Element Formulations

R. V. Sabariego [1], P. Dular [1,2], C. Geuzaine [1] and J. Gyselinck [3]

[1] Dept. of Electrical Engineering and Computer Science (ACE), University of Liège, Belgium
[2] Fonds de la Recherche Scientifique - F.R.S.-FNRS, Belgium
[3] Dept. of Bio-, Electro- and Mechanical Systems (BEAMS), Université Libre de Bruxelles (ULB), Belgium

This paper deals with time-domain surface-impedance boundary conditions in computational magnetodynamics considering two dual finite-element formulations and a nonlinear magnetic constitutive law. Based on the resolution of the 1-D eddy-current problem in a semi-infinite slab, the massive conducting region is accounted for by choosing a number of exponentially decreasing trigonometric basis functions covering the relevant frequency range of the application in hand. Herein the method is elaborated for the magnetic-vector-potential formulation and the magnetic-field formulation. Results for both formulations are compared and validated on two-dimensional linear and nonlinear test cases.

Index Terms— **Surface-impedance boundary conditions, finite-element methods, magnetodynamics, time-domain analysis**

I. Introduction

SURFACE-impedance boundary conditions (SIBCs) are widely applied in frequency-domain magnetodynamic problems for removing the massive conducting regions from the computation domain and greatly reducing the computational cost. The surface-impedance concept provides approximate relations between the fields at the surface of a massive conducting domain when their variation of along this surface can be assumed to be small compared to the one in the normal direction. The field derivatives in the directions tangential to the surface may be thus neglected compared to the normal derivative and the original governing 3-D equation in the conducting region can be reduced to a 1-D equation. This 1-D equation relates the tangential components of the electric and magnetic field at the surface of the conducting region and allows to avoid the discretization of its volume. A necessary condition is that at the considered frequency the skin depth is sufficiently small compared to the depth or curvature of the conducting region. Several refinements concerning the surface curvature, the corners and edges [1], [2] but also the material saturation [3] can be found in the literature.

The few time-domain extensions proposed to date are mostly based on Fourier transform techniques [2], [4], or on the iterative coupling between the main 3-D finite element (FE) model and a large number of 1-D FE calculations (with classical nodal basis functions) [5].

In [6], the authors proposed a time-domain approach for the magnetic-vector-potential formulation. The method relies on the spatial distribution of a 1-D eddy-current problem by means of dedicated basis functions derived from the analytical frequency-domain solution. In this paper this approach is extended for the magnetic-field formulation. Expressions for energy-related quantities in terms of the surface field distribution are also developed. Results of the two considered dual formulations are compared and validated on an application example with both linear and nonlinear materials.

Manuscript received December 23, 2009. Corresponding author: R. V. Sabariego (e-mail: r.sabariego@ulg.ac.be).

II. 1-D eddy-current problem in semi-infinite slab

Let us consider a magnetodynamic problem in a semi-infinite slab Ω_m ($0 \leq x \leq \infty$), with the flux density (or induction) $\underline{b}(x,t)$ and the magnetic field $\underline{h}(x,t)$ parallel to the z-axis, the current density $\underline{j}(x,t)$ and the electric field $\underline{e}(x,t)$ parallel to the y-axis. We are first concerned with linear isotropic and homogeneous media, i.e. the conductivity σ (resistivity $\rho = 1/\sigma$) and the permeability μ (reluctivity $\nu = 1/\mu$) are constant scalars. Under these hypotheses, the Ampère law and the Faraday law can be written as

$$\operatorname{curl}(\nu \operatorname{curl} \underline{a}) = -\sigma\, \partial_t\, \underline{a}\,, \quad \operatorname{curl}(\rho \operatorname{curl} \underline{h}) = -\mu\, \partial_t\, \underline{h}\,, \quad (1)$$

with constitutive laws $\underline{b} = \mu\, \underline{h}$, $\underline{j} = \sigma \underline{e}$ and where $\underline{a}$ is the magnetic vector potential ($\underline{b} = \operatorname{curl} \underline{a}$, $\underline{j} = -\sigma \partial_t \underline{a}$).

Due to the symmetry of the problem, all derivatives with respect to y and z vanish and equations (1) amount to the following 1-D partial differential equations:

$$\partial_x^2 a(x,t) \;=\; \sigma\mu\, \partial_t a(x,t)\,, \qquad a(x=\infty,t) = 0\,, \quad (2)$$

$$\partial_x^2 h(x,t) \;=\; \sigma\mu\, \partial_t h(x,t)\,, \qquad h(x=\infty,t) = 0\,, \quad (3)$$

where $a(x,t)$ is the $y-$component of $\underline{a}$ and $h(x,t)$ the $z-$component of $\underline{h}$. The boundary conditions at infinity ($x = \infty$) ensure the uniqueness of $a(x,t)$ and the physical behavior of $h(x,t)$. The flux in the semi-infinite slab (or the magnetomotive force) may be imposed via the boundary value $a(x=0,t)$ (or $h(x=0,t)$).

Let us consider e.g. the sinusoidal steady-state solution of (3) at frequency f (pulsation $\omega = 2\pi f$), with boundary condition $h(x=0,t) = \hat{h}\, \cos(\omega t + \phi)$:

$$\begin{aligned} h(x,t) \;&=\; \hat{h}\; e^{-x/\delta} \cos(x/\delta - \omega t - \phi) \\ &=\; \hat{h}\, \cos(\omega t + \phi)\; e^{-x/\delta} \cos(x/\delta) \\ &+\; \hat{h}\, \sin(\omega t + \phi)\; e^{-x/\delta} \sin(x/\delta)\,, \end{aligned} \quad (4)$$

with $\delta = \sqrt{2/(\mu\sigma\omega)}$ the skin depth and ϕ an arbitrary phase.

Using the complex notation (symbols in bold, imaginary unit $\sqrt{-1}$ denoted by $\boldsymbol{\imath}$), we rewrite (4) as follows

$$h(x,t) \;=\; \Re\big(\hat{h}\, e^{-\frac{1+\boldsymbol{\imath}}{\delta}\, x}\, e^{\boldsymbol{\imath}\,(\omega t + \phi)}\big)\,, \quad \boldsymbol{h}(x) \;=\; \hat{h}\, e^{\boldsymbol{\imath}\,\phi}\; e^{-\frac{1+\boldsymbol{\imath}}{\delta}\, x}\,, \quad (5)$$

which further leads to a relation at the surface $x = 0$:

$$\partial_x \boldsymbol{h}\Big|_{x=0} \;=\; -\frac{1+\imath}{\delta}\,\boldsymbol{h}(x=0)\,. \tag{6}$$

It is this equation that is at the heart of the classical frequency-domain SIBC approach. Note that the expressions in terms of the magnetic vector potential are straightforwardly obtained by substituting h by a in (4)–(6).

A. Basis functions for the low-order time-domain model

The choice of basis functions is motivated by the solution of the 1-D eddy-current problem (4) [6]. For a given time-domain problem, a set of n skin depths δ_k, $1 \le k \le n$, can be preset accounting for the frequency content of the magnetic fields in the problem in hand and the wished accuracy. We define thus the following $2n$ basis functions:

$$\alpha_{c1}(x) = e^{-x/\delta_1}\cos(x/\delta_1)\,, \tag{7}$$

$$\alpha_{ck}(x) = e^{-x/\delta_k}\cos(x/\delta_k) - \alpha_{c1}(x)\,,\quad 2 \le k \le n\,, \tag{8}$$

$$\alpha_{sk}(x) = e^{-x/\delta_k}\sin(x/\delta_k)\,,\quad 1 \le k \le n\,. \tag{9}$$

Note that all basis functions vanish at the boundary except the first one, i.e. $\alpha_{c1}(x=0) = 1$.

The associated expansions of $a(x,t)$ and $h(x,t)$ are written in matrix form as:

$$a(x,t) = [A(t)]^T[\alpha(x)]\,,\; h(x,t) = [H(t)]^T[\alpha(x)]\,, \tag{10 a b}$$

with the $2n \times 1$ matrices $[A(t)]$, $[H(t)]$ and $[\alpha(x)]$ given by

$$[A(t)] \;=\; [a_{c1}(t)\;\ldots\;a_{cn}(t)\;a_{s1}(t)\;\ldots\;\;a_{sn}(t)]^T\,, \tag{11}$$

$$[H(t)] \;=\; [h_{c1}(t)\;\ldots\;h_{cn}(t)\;h_{s1}(t)\;\ldots\;\;h_{sn}(t)]^T\,, \tag{12}$$

$$[\alpha(x)] \;=\; [\alpha_{c1}(x)\;\ldots\;\alpha_{cn}(x)\;\alpha_{s1}(x)\;\ldots\;\;\alpha_{sn}(x)]^T\,. \tag{13}$$

B. 1-D magnetic-vector-potential formulation

The variational form of the second-order partial differential equation (2) characterizing the 1-D eddy-current problem in the infinite slab Ω_m is given by

$$(\nu\,\partial_x a, \partial_x\alpha')_{\Omega_m} + \partial_t(\sigma\,a, \alpha')_{\Omega_m} = 0\,, \tag{14}$$

where $(\cdot\,,\cdot)_{\Omega_m}$ denotes an integral in Ω_m of the scalar product of their arguments; α' is the test function for a.

The FE discretization of (14) by means of N basis functions $\alpha_i(x)$, $0 \le x < \infty$, $1 \le i \le N$, for a and α', leads thus to the following system of first-order differential equations:

$$\nu\,[\mathcal{S}][A(t)] + \sigma\,[\mathcal{M}]\,\partial_t[A(t)] \;=\; 0\,, \tag{15}$$

where the elements of the matrices $[S]$ and $[M]$ are given by

$$\mathcal{S}_{ij} = \int_0^\infty \partial_x\alpha_i(x)\,\partial_x\alpha_j(x)\,dx\,, \tag{16}$$

$$\mathcal{M}_{ij} = \int_0^\infty \alpha_i(x)\,\alpha_j(x)\,dx\,. \tag{17}$$

Further, the system (15) is discretized in time by means of the so-called $\theta-$scheme, which amounts to backward Euler with $\theta = 1$ and to Crank-Nicolson with $\theta = 0.5$. A system of algebraic equations is obtained for each time-step from t_i to $t_{i+1} = t_i + \Delta t$.

The elements of $[\mathcal{S}]$ and $[\mathcal{M}]$ can be evaluated analytically considering the following relations [6]:

$$\begin{aligned}\int_0^\infty e^{-x/\delta_k}\,e^{-x/\delta_l}\begin{bmatrix}\cos(x/\delta_k)\,\cos(x/\delta_l)\\ \cos(x/\delta_k)\,\sin(x/\delta_l)\\ \sin(x/\delta_k)\,\sin(x/\delta_l)\end{bmatrix}dx\\ =\;\frac{\delta_k\,\delta_l}{2\,(\delta_k+\delta_l)\,(\delta_k^2+\delta_l^2)}\begin{bmatrix}\delta_k^2+\delta_l^2+\delta_k\delta_l\\ \delta_k^2\\ \delta_k\,\delta_l\end{bmatrix}.\end{aligned} \tag{18}$$

Energy-related quantities: The positive-definite quadratic forms associated to matrices $[\mathcal{S}]$ and $[\mathcal{M}]$ are the instantaneous magnetic energy density $w^a(t)$ and the instantaneous eddy-current loss density $p^a(t)$ (in joules and watts per square meter of surface of the boundary respectively):

$$w^a(t) \;=\; \nu\,[A(t)]^T\,[\mathcal{S}]\,[A(t)]\,, \tag{19}$$

$$p^a(t) \;=\; \sigma\,\partial_t[A(t)]^T\,[\mathcal{M}]\,\partial_t[A(t)]\,. \tag{20}$$

Nonlinear case: For nonlinear isotropic materials, the 1-D variational formulation reads:

$$(h(b), \partial_x\alpha')_{\Omega_m} + \partial_t(\sigma\,a, \alpha')_{\Omega_m} = 0\,, \tag{21}$$

with constitutive law $h = h(b)$ and $b(x,t) = [A(t)]^T[\partial_x\alpha(x)]$.

The nonlinear algebraic equations that result from the time discretization of (21) can be solved by the Newton-Raphson scheme [7]. Subsequent iterations of the Newton-Raphson scheme produce increments $[\Delta A]_k$, $k = 1, 2\ldots$, via the solution of a system of linearized equations, i.e.

$$[J]_{k-1}\,[\Delta A]_k \;=\; [H]_{k-1} + \ldots\,. \tag{22}$$

The Jacobian matrix $[\mathcal{J}]$ and the associated column matrix $[H]$, which is part of the residue, are given by:

$$\mathcal{J}_{ij} = \int_0^\infty \frac{d\,h}{d\,b}\;\partial_x\alpha_i(x)\,\partial_x\alpha_j(x)\,dx\,, \tag{23}$$

$$H_i = \int_0^\infty h(b)\;\partial_x\alpha_i(x)\,dx\,. \tag{24}$$

The differential reluctivity $\frac{d\,h}{d\,b}$ in (23) can also be written in terms of $\nu(b^2)$ and its derivative with respect to b^2:

$$\frac{d\,h}{d\,b} = \nu + 2\,b^2\,\frac{d\,\nu}{d\,b^2}\,. \tag{25}$$

One has to resort to numerical integration for evaluating $[J]$ and $[H]$ at each NR-iteration [7].

C. 1-D magnetic-field formulation

The variational form of (3) is written as

$$(\rho\,\partial_x h, \partial_x\alpha')_{\Omega_m} + \partial_t(\mu\,h, \alpha')_{\Omega_m} = 0\,, \tag{26}$$

with α' the test function for h.

Analogously to the magnetic-vector-potential formulation, the spatial discretization of (26) by means of N basis functions $\alpha_i(x)$, $0 \le x < \infty$, $1 \le i \le N$, for h and α', leads to the following system of first-order differential equations:

$$\rho\,[\mathcal{S}][H(t)] + \mu\,[\mathcal{M}]\,\partial_t[H(t)] \;=\; 0\,, \tag{27}$$

where the elements of the matrices $[\mathcal{S}]$ and $[\mathcal{M}]$ are given by (16) and (17), respectively. A system of algebraic equations is further obtained for each time step by discretizing (27) in time (e.g. $\theta-$scheme).

Energy-related quantities: The instantaneous magnetic energy density $w^h(t)$ and the instantaneous eddy-current loss density $p^h(t)$ are given by:

$$w^h(t) \;=\; \mu\,[H(t)]^T\,[\mathcal{M}]\,[H(t)]\,, \tag{28}$$

$$p^h(t) \;=\; \rho\,[H(t)]^T\,[\mathcal{S}]\,[H(t)]\,. \tag{29}$$

Nonlinear case: The variational formulation of the 1-D eddy-current problem is written as:

$$(\rho\,\partial_x h, \partial_x \alpha')_{\Omega_m} + \partial_t (b(h), \alpha')_{\Omega_m} = 0\,, \tag{30}$$

with nonlinear constitutive law $b = b(h)$.

The time discretization of (30) leads to a system of nonlinear algebraic equations to be solved by e.g. the Newton-Raphson scheme. Subsequent iterations of the Newton-Raphson scheme produce increments $[\Delta B]_k$, $k = 1, 2\ldots$, via the solution of a system of linearized equations, i.e.

$$[\mathcal{J}]_{k-1}\,[\Delta B]_k \;=\; [B]_{k-1} + \ldots\,. \tag{31}$$

The Jacobian matrix $[\mathcal{J}]$ and the column matrix $[B]$ are:

$$\mathcal{J}_{ij} = \int_0^\infty \frac{d\,b}{d\,h}\;\alpha_i(x)\,\alpha_j(x)\,dx\,, \tag{32}$$

$$B_i = \int_0^\infty b(h)\;\alpha_i(x)\,dx\,. \tag{33}$$

The differential permeability $\frac{d\,b}{d\,h}$ in (32) can also be written in terms of $\mu(h^2)$ and its derivative with respect to h^2:

$$\frac{d\,b}{d\,h} = \mu + 2\,h^2\,\frac{d\,\mu}{d\,h^2}\,. \tag{34}$$

III. Integration in FE model

Let us consider now a magnetodynamic problem in a bounded domain $\Omega = \Omega_c \cup \Omega_c^C \in \mathbb{R}^3$ with boundary $\Gamma = \Gamma_h \cup \Gamma_e$, which is composed of two complementary parts Γ_h and Γ_e (connected or not). The conductive and non-conductive parts of Ω are denoted by Ω_c and Ω_c^C, respectively. Source inductors with given current density $\underline{j}_s$ constitute domain $\Omega_s \subset \Omega_c^C$. The SIBC method will be applied to a massive sub-domain Ω_m of Ω_c with boundary $\partial\Omega_m \subset \Gamma$.

A. Magnetic-vector-potential formulation

The magnetic-vector-potential ($\underline{a}-$)formulation is obtained from the weak form of the Ampère law ($\mathrm{curl}\,\underline{h} = \underline{j}$):

$$(\nu\,\mathrm{curl}\,\underline{a}, \mathrm{curl}\,\underline{a}')_\Omega + (\sigma\,\partial_t \underline{a}, \underline{a}')_{\Omega_c} + \langle \underline{n}\times\underline{h}, \underline{a}'\rangle_{\Gamma_h} = (\underline{j}_s, \underline{a}')_{\Omega_s}\,, \tag{35}$$

where $(\cdot\,,\cdot)_\Omega$ and $\langle\cdot\,,\cdot\rangle_{\Gamma_h}$ are the integrals on the domain Ω and on the boundary Γ_h, respectively, of the product of the two arguments; $\underline{n}$ is the outward normal on Γ_h.

When applying the classical SIBC approach, the massive conductive region Ω_m is extracted from Ω_c, preserving only a boundary term on $\partial\Omega_m$ in (35), i.e.

$$\begin{aligned}(\nu\,\mathrm{curl}\,\underline{a}, \mathrm{curl}\,\underline{a}')_{\Omega\setminus\Omega_m} + (\sigma\,\partial_t \underline{a}, \underline{a}')_{\Omega_c\setminus\Omega_m} \\ + \langle \underline{n}\times\underline{h}, \underline{a}'\rangle_{\Gamma_h\cup\partial\Omega_m} = (\underline{j}_s, \underline{a}')_{\Omega_s}\,.\end{aligned} \tag{36}$$

In the frequency domain, the surface integral of the tangential magnetic field $\underline{n}\times\underline{h}$ on $\partial\Omega_m$ is then expressed in terms of the tangential electric field $\underline{n}\times\underline{e}$ thanks to the classical SIBC, the general form of (6):

$$\underline{n}\times\underline{e} = \frac{1+\imath}{\sigma\,\delta}\left(\underline{n}\times(\underline{h}\times\underline{n})\right). \tag{37}$$

From (37) and $\underline{e} = -\partial_t \underline{a}$, the surface integral on $\partial\Omega_m$ in (36) reads:

$$\langle \underline{n}\times\underline{h}, \underline{a}'\rangle_{\partial\Omega_m} = \langle -\nu\frac{1+\imath}{\delta}\,\underline{a}_t\,, \underline{a}'\rangle_{\partial\Omega_m}\,, \tag{38}$$

where $\underline{a}_t = \underline{n}\times(\underline{a}\times\underline{n})$ denotes the magnetic vector potential tangential to $\partial\Omega_m$.

The surface integral on $\partial\Omega_m$ can also be derived from the two volume integrals in Ω_m, which are further reduced to surface integrals, as explained hereafter. If we consider (35) restricted to domain Ω_m, where $\underline{j}_s = 0$, we can write:

$$\langle \underline{n}\times\underline{h}, \underline{a}'\rangle_{\partial\Omega_m} = -(\nu\,\mathrm{curl}\,\underline{a}, \mathrm{curl}\,\underline{a}')_{\Omega_m} - (\sigma\,\partial_t \underline{a}, \underline{a}')_{\Omega_m}\,. \tag{39}$$

Hereto we consider a local coordinate system xyz on $\partial\Omega_m$, with the x-axis parallel to $\underline{n}$ and inward Ω_m. Further ignoring the finite depth of Ω_m and the nonzero curvature of $\partial\Omega_m$, we write the magnetic vector potential in the transformed domain Ω_m as: $\underline{a} = \underline{a}_t(y,z,t)\,p(x)$, where $\underline{a}_t$ is tangential to $\partial\Omega_m$ and $p(x)$ is differentiable with respect to x ($0 \le x < \infty$). The two volume integrals in (39) are then worked out accordingly:

$$\begin{aligned}(\nu\,\mathrm{curl}\,\underline{a}, \mathrm{curl}\,\underline{a}')_{\Omega_m} &= (\nu\,\mathrm{curl}\,(\underline{a}_t\,p), \mathrm{curl}\,(\underline{a}'_t\,p'))_{\Omega_m} \\ &= (\nu(p\,\mathrm{curl}\,\underline{a}_t - \underline{a}_t\times\mathrm{grad}\,p), p'\,\mathrm{curl}\,\underline{a}'_t - \underline{a}'_t\times\mathrm{grad}\,p')_{\Omega_m} \\ &= \langle \underline{a}_t, \underline{a}'_t\rangle_{\partial\Omega_m}\cdot\nu\int_0^\infty \partial_x p\,\partial_x p'\,dx\,,\end{aligned} \tag{40}$$

$$\begin{aligned}(\sigma\,\partial_t \underline{a}, \underline{a}')_{\Omega_m} &= (\sigma\,\partial_t(\underline{a}_t\,p), \underline{a}'_t\,p')_{\Omega_m} \\ &= \langle \partial_t \underline{a}_t, \underline{a}'_t\rangle_{\partial\Omega_m}\cdot\sigma\int_0^\infty p\;p'\,dx\,.\end{aligned} \tag{41}$$

The domain $\Omega\setminus\Omega_m$, its boundary and the weak form (36) can be discretized by Whitney edge elements, leading to a system of linear first-order differential equations in terms of the degrees of freedom of $\underline{a}$ (circulation of $\underline{a}$ on the edges of the FE mesh) [8]. Furthermore, considering the n pairs of basis functions $\alpha_{ck}(x)$ and $\alpha_{sk}(x)$ for the space discretization of $p(x)$ and test functions $p'(x)$, the integration along the x-axis in (40) and (41) produces the elements of (16) and (17), respectively.

The number of spatial degrees of freedom of $\underline{a}$ on $\partial\Omega_m$ (no volume discretization) is thus equal to the number of edges on the surface $\partial\Omega_m$ multiplied by $2n$.

B. Magnetic-field formulation

The general expression of the magnetic field $\underline{h}$ in Ω is given by $\underline{h} = \underline{h}_s + \underline{h}_r$, where $\underline{h}_s$ is a source field satisfying $\mathrm{curl}\,\underline{h}_s = \underline{j}_s$ in Ω_s, and $\underline{h}_r$ is the reaction field. The magnetic-field ($\underline{h}-$)formulation is obtained from the weak form of the Faraday law ($\mathrm{curl}\,\underline{e} = -\partial_t\,\underline{b}$). It reads:

$$\partial_t(\mu\,\underline{h}, \underline{h}')_\Omega + (\rho\,\mathrm{curl}\,\underline{h}, \mathrm{curl}\,\underline{h}')_{\Omega_c} + \langle \underline{n}\times\underline{e}, \underline{h}'\rangle_{\Gamma_e} = 0\,. \tag{42}$$

As previously mentioned, the SIBC method in the frequency domain amounts to replacing the massive conducting domain Ω_m by an impedance condition (37) at its boundary via the surface integral term in (43), i.e.

$$\partial_t(\mu\,\underline{h},\underline{h}')_{\Omega\setminus\Omega_m} + (\rho\,\mathrm{curl}\,\underline{h},\mathrm{curl}\,\underline{h}')_{\Omega_c\setminus\Omega_m} + \langle\underline{n}\times\underline{e},\underline{h}'\rangle_{\Gamma_e\cup\partial\Omega_m} = 0\,, \qquad (43)$$

where the surface integral on $\partial\Omega_m$ is now written in terms of $\underline{h}_t = \underline{n}\times(\underline{h}\times\underline{n})$, the magnetic field tangential to $\partial\Omega_m$, $\underline{h}_t = \underline{n}\times(\underline{h}\times\underline{n})$. The frequency SIBC is thus given by:

$$\langle\underline{n}\times\underline{e},\underline{h}'\rangle_{\partial\Omega_m} = \langle\rho\frac{1+\imath}{\delta}\,\underline{h}_t\,,\underline{h}'\rangle_{\partial\Omega_m}\,. \qquad (44)$$

Analogously to the $\underline{a}-$formulation treatment, the proposed time-domain approach amounts to expressing the surface integral on $\partial\Omega_m$ by means of two volume integrals. From (43) restricted to Ω_m, it follows:

$$\langle\underline{n}\times\underline{e},\underline{h}'\rangle_{\partial\Omega_m} = -\partial_t(\mu\,\underline{h},\underline{h}')_{\Omega_m} - (\rho\,\mathrm{curl}\,\underline{h},\mathrm{curl}\,\underline{h}')_{\Omega_m}\,. \qquad (45)$$

Further, ignoring the finite depth of Ω_m and the curvature of $\partial\Omega_m$, we can write the local magnetic field in Ω_m as $\underline{h} = \underline{h}_t(y,z,t)\,p(x)$, with $\underline{h}_t$ tangential to $\partial\Omega_m$ and $p(x)$ differentiable with respect to x ($0 \le x < \infty$). The two volume integrals considered in Ω_m (45) are thus reduced to the following surface integrals:

$$\begin{aligned}\partial_t(\mu\,\underline{h},\underline{h}')_{\Omega_m} &= \partial_t(\mu\,\underline{h}_t\,p,\underline{h}'_t\,p')_{\Omega_m}\\ &= \partial_t\langle\underline{h}_t,\underline{h}'_t\rangle_{\partial\Omega_m}\cdot\,\mu\int_0^\infty p\;p'\,dx\,,\end{aligned} \qquad (46)$$

$$\begin{aligned}(\rho\,\mathrm{curl}\,\underline{h},\mathrm{curl}\,\underline{h}')_{\Omega_m} &= (\rho\,\mathrm{curl}\,(\underline{h}_t\,p),\mathrm{curl}\,(\underline{h}'_t\,p))_{\Omega_m}\\ &= (\rho\,(p\,\mathrm{curl}\,\underline{h}_t - \underline{h}_t\times\mathrm{grad}\,p),p'\,\mathrm{curl}\,\underline{h}'_t - \underline{h}'_t\times\mathrm{grad}\,p')_{\Omega_m}\\ &= \langle\underline{h}_t,\underline{h}'_t\rangle_{\partial\Omega_m}\cdot\,\rho\int_0^\infty \partial_x p\;\partial_x p'\,dx\,.\end{aligned} \qquad (47)$$

Discretizing (43) with Whitney elements and basis functions $p(x)$ and $p'(x)$ with $\alpha_{ck}(x)$ and $\alpha_{sk}(x)$, we obtain the system of differential equations to solve.

IV. Application example

The 2-D application example concerns a conducting cylinder (circular cross-section with radius $R = 10\,\mathrm{cm}$) placed inside an inductor (rectangular cross-section) with imposed current. Only one quarter of the geometry is modeled (Fig. 1).

We consider 1) a copper cylinder ($\sigma = 60\,\mathrm{MS/m}$, $\mu = \mu_0 = 4\pi\,10^{-7}$ H/m), i.e. a linear non-magnetic conducting material; 2) a steel cylinder ($\sigma = 2\,\mathrm{MS/m}$, $\nu(b^2) = 100 + 10\exp(1.8\,b^2)$ with b in T and ν in m/H), i.e. a magnetic conducting material with nonlinear constitutive law.

The classical $\underline{a}-$ and $\underline{h}-$formulations with a very fine discretization of the cylinder near its surface provide an accurate reference solution for very small δ/R ratios (Fig. 1). When applying the SIBC, only the mesh outside the cylinder is effectively considered. A transformation method is used to account for the extension of space to infinity.

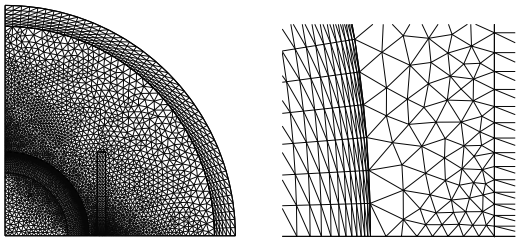

Fig. 1. FE model and mesh (1/4 of geometry) and detail of the FE mesh (the width of the outer layer of elements in the disk is equal to 0.3 mm, i.e. 0.3% of the radius R)

A. Linear case

Two typical flux patterns obtained with the $\underline{a}-$formulation are depicted in Fig. 2. As it will be shown hereafter, the SIBC approximation is sufficiently accurate for $\delta/R = 0.1$ (right) but not for $\delta/R = 0.5$ (left).

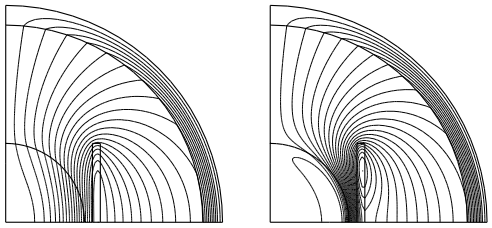

Fig. 2. Flux pattern (in phase with imposed sinusoidal current) with $\delta/R = 0.5$ (left) and $\delta/R = 0.1$ (right)

The classical frequency-domain SIBCs (6) are first applied to our test case, with imposed sinusoidal current of unit amplitude and with δ/R ranging from 0.01 ($f = 4.2\,\mathrm{kHz}$) up to 1.5 ($f = 0.19\,\mathrm{Hz}$) approximately. Fig. 3 shows the real and imaginary part of flux linkage of the inductor (normalized with the flux at 0 Hz) obtained with the $\underline{a}-$ and $\underline{h}-$formulations, fine reference models and classical SIBCs. (Note that the imaginary part of the flux corresponds to the eddy-current losses in the cylinder, whereas its real part corresponds to the magnetic energy in the complete model.) One can conclude that the SIBC approaches are accurate for $\delta/R < 0.1$.

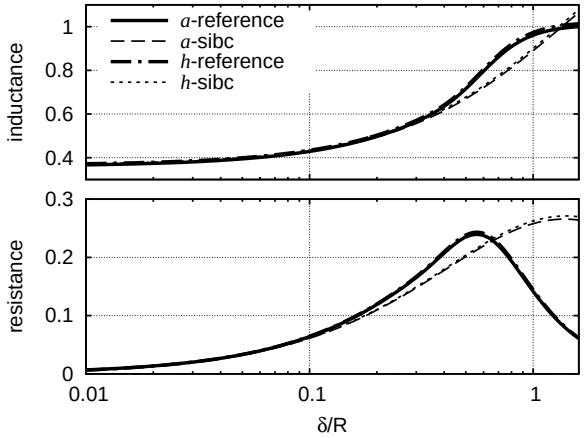

Fig. 3. Real and imaginary part of normalized flux linkage as a function of skin depth, calculated with fine models and exact SIBCs

For the sake of validation, we apply the proposed low-

order SIBC approximation in the frequency domain, with $f_1 = 1\,\text{kHz}$ ($\delta_1/R = 0.02$) and further discrete frequencies being odd harmonics of f_1, i.e. $f_k/f_1 = 2k-1$ with $1 \leq k \leq n$ (or in terms of the skin depths $\delta_k/\delta_1 = \sqrt{2k-1}$). Fig. 4 shows the real and imaginary part of the normalized flux obtained with n equal to 1, 2 and 3 for both dual formulations.

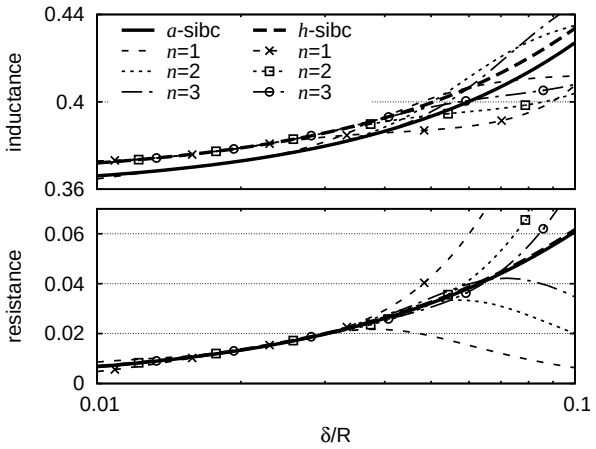

Fig. 4. Real and imaginary part of normalized flux linkage as a function of skin depth, calculated with fine model, exact SIBC and time-domain SIBCs

A trapezoidal current varying between 1 and -1 at frequency $f = 1\,\text{kHz}$ is next considered. Time-stepping simulations are carried out. One period $T = 1/f = 1\,\text{ms}$ is discretized with a $\theta-$scheme and time step $\Delta t = T/240$.

The tangential induction and current density in a point at the surface of the cylinder (cylindrical coordinates $(R, \frac{\pi}{4})$) are shown in Fig. 5 for the first fundamental period (1 ms). Results obtained with both reference formulations are compared with the corresponding SIBC approximations. For the low-order SIBC approaches, odd harmonics of $f_1 = 1\,\text{kHz}$ are considered.

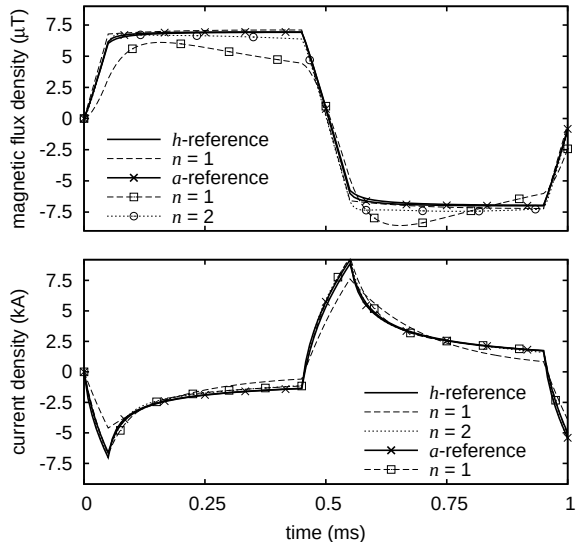

Fig. 5. Induction and current density at point $(R, \frac{\pi}{4})$ versus time obtained with dual fine models and time-domain SIBC approaches

For a given SIBC solution f^n, with reference f^{ref} (fine model), we define its relative error as:

$$\text{relative error} := \frac{f^{ref} - f^n}{\max\left(f^{ref}\right)}\,. \tag{48}$$

The relative error (48) made when computing the induction and current density at point $(R, \frac{\pi}{4})$ by means of the time-domain SIBC approximations is depicted in Fig. 6 as well. Note that the results obtained with the low-order SIBC approximations converge faster for the induction $\underline{b}$ with the $h-$formulation and for the current $\underline{j}$ with the $a-$formulation. Indeed, the induction $\underline{b}$ and the current density $\underline{j}$ are primary local quantities in the $h-$ and $a-$formulations, respectively, obtained without further spatial derivation ($\underline{b} = \text{curl}\,\underline{a}$ with the $a-$formulation and $\underline{j} = \text{curl}\,\underline{h}$ with the $h-$formulation).

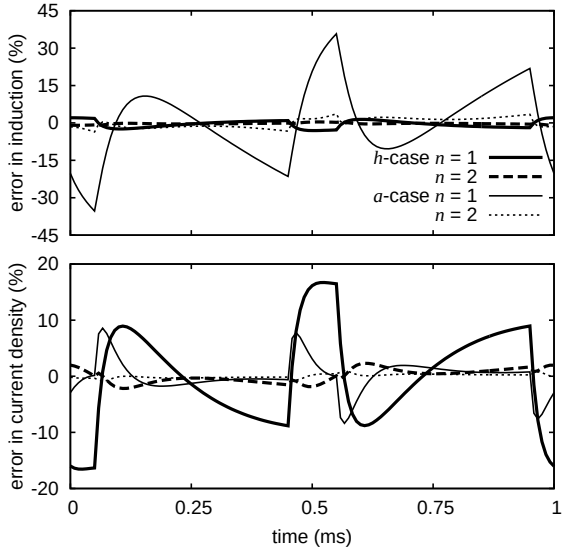

Fig. 6. Relative error (%) of induction (up) and current density (down) at point $(R, \frac{\pi}{4})$ made with the time-domain SIBC approximations ($n = 1, 2$)

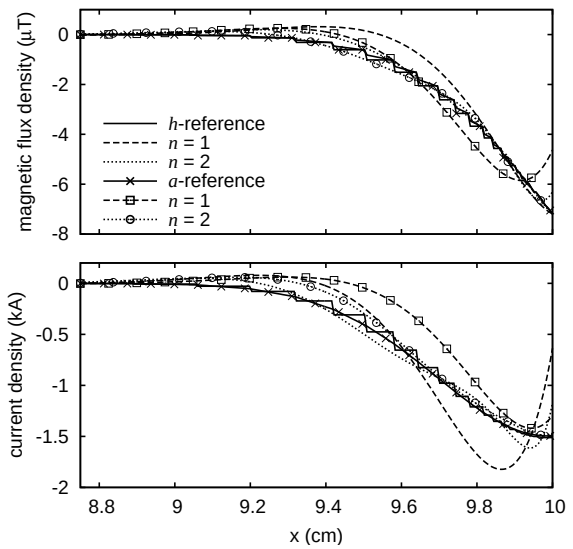

Fig. 7. Variation of the induction (up) and current density (down) inside the cylinder versus x obtained with dual fine models and time-domain SIBC approaches

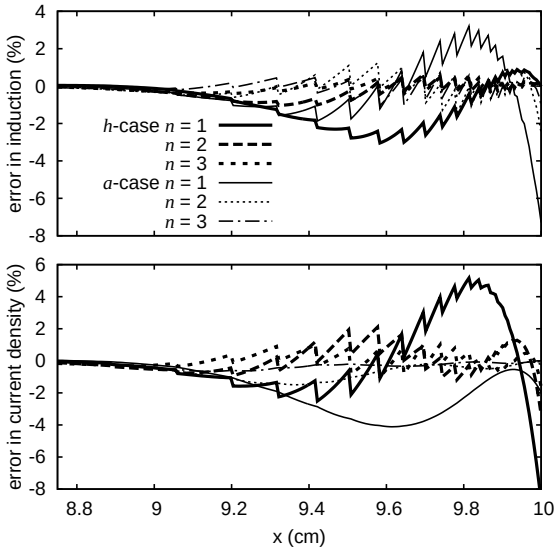

Fig. 8. Relative error (%) of induction (up) and current density (down) inside the cylinder made with the time-domain SIBC approximations ($n = 1, 2, 3$)

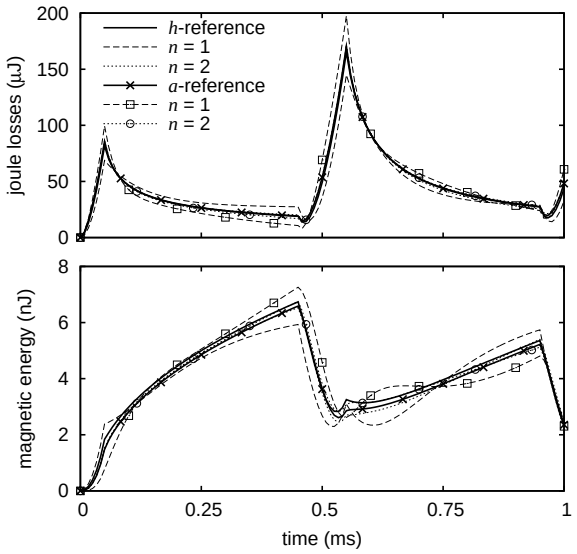

Fig. 9. Joule losses (up) and magnetic energy (down) in the cylinder versus time obtained with dual fine models and time-domain SIBC approximations ($n = 1, 2$)

The variation of the magnetic flux and current density inside the cylinder (from $R - R/8$ to its boundary at $(R, \pi/4)$, time-step 45, $t = 0.1875\,\text{ms}$) is depicted in Fig. 7; the ensuing relative error (48) is shown in Fig. 8. For the SIBC approach, these values are computed in a post-processing stage, using the dedicated basis functions (7)-(9), their derivatives and the tangential fields at the cylinder surface for a given time-step. The approximation clearly improves with n.

The magnetic energy and the joule losses in the cylinder are calculated during the first period with the fine model (without SIBC) and the low-order SIBC ($n = 1, 2$), see Fig. 9. The corresponding relative error (48) is depicted in Fig. 10. A very good convergence of the SIBC results towards the reference results for both formulations is clearly observed in Fig. 10. Note that the results given by the low-order SIBC approximations convergence equally faster, independently of the formulation considered, for these two global quantities.

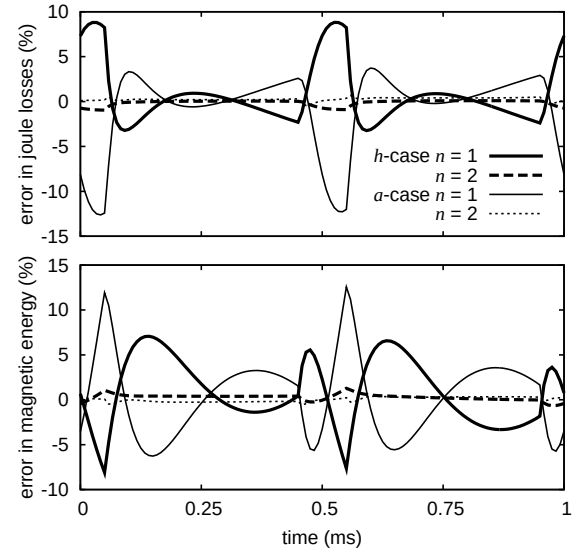

Fig. 10. Relative error (%) of joule losses (up) and magnetic energy (down) obtained with the time-domain SIBC approximations ($n = 1, 2$)

B. Nonlinear case

Let us consider now an imposed sinusoidal current (50 Hz, amplitude 6000 At). In this section, only results obtained with the $a-$formulation are shown.

We adopt a low order approximation of the SIBC with $f_1 = 50\,\text{kHz}$ and further discrete frequencies being odd multiples of f_1, as previously defined. The skin depth δ_1 is given by a reluctivity $\nu = 674\,\text{m/H}$ which corresponds to $b = 1.5\,\text{T}$ (nonlinear law).

The induction at the point of the surface of the conducting cylinder closest to the inductor is depicted in Fig. 11. The relative error (48) is shown in Fig. 12 as well.

Figs. 13 and 14 show the induction at a point on the x-axis halfway between the cylinder and the inductor and the relative error, respectively.

One clearly observes the saturation and the effect of the eddy currents. An excellent agreement is observed between the flux waveforms obtained with the reference FE model and

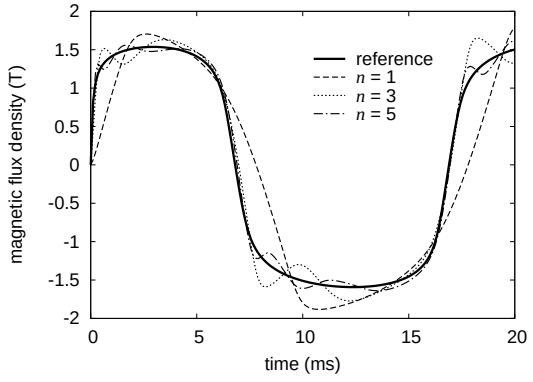

Fig. 11. Induction waveform obtained with reference model and the SIBC approach ($n = 1, 3, 5$) at the surface of the cylinder

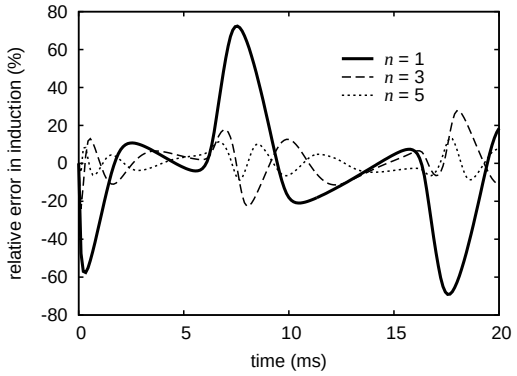

Fig. 12. Relative error (%) of induction at the surface of the cylinder made with the SIBC approach ($n = 1, 3, 5$)

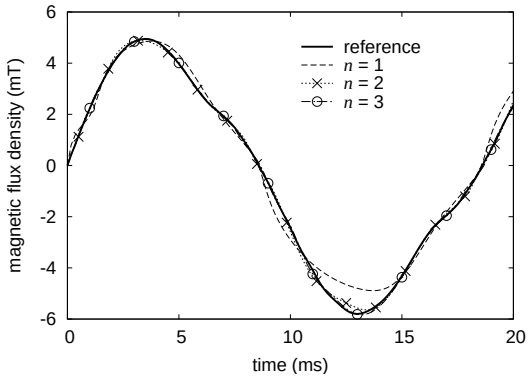

Fig. 13. Induction waveform obtained with reference model and the SIBC approach ($n = 1, 2, 3$) at a point between the cylinder and the inductor

the SIBC approach with $n = 3$. Even though in both cases, the approximation clearly improves with n, more terms are needed for increasing the precision at the surface of the cylinder.

V. Conclusions

A low-order time-domain SIBC approach has been elaborated for two dual finite element formulations considering either a linear or a nonlinear constitutive law for the conducting material. The proposed approach is based on the resolution of the 1-D eddy-current problem in a massive conducting region (semi-infinite slab) by considering a reduced number of pairs of exponentially decreasing and frequency (skin depth) dependent trigonometric basis functions. For a given time-domain problem, a set of skin depths can be preset accounting for the frequency content of the magnetic fields, the level of saturation and accuracy required. The choice of the associated discrete skin depths is thus application dependent but the stiffness and conductivity matrices to be evaluated for the application are essentially a function of the skin-depth ratios. The additional number of unknowns on the boundary of the conducting domain is thus very limited. When dealing with nonlinear materials, the system of nonlinear algebraic equations is solved by means of the Newton-Raphson scheme.

The method provides a good compromise between computational cost and accuracy. Indeed, adding a sufficiently large number of magnetic-vector-potential or magnetic field components on the boundary of the conducting domain, a very high precision can be achieved.

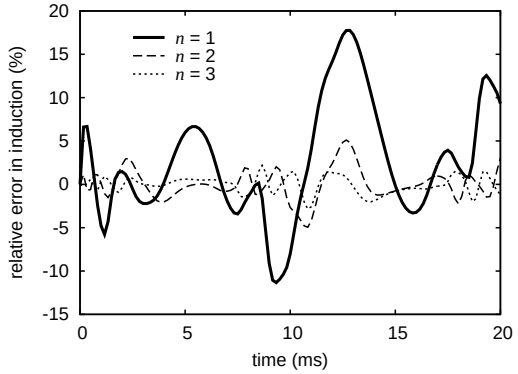

Fig. 14. Relative error in percent (%) of induction at a point between the cylinder and the inductor made with the SIBC approach ($n = 1, 2, 3$)

Future research concerns the use of higher order SIBCs as starting point to handle edges and curvatures that are comparable to the skin depth.

Acknowledgment

This work was partly supported by the Belgian Science Policy (IAP P6/21) and the Walloon region (WIST2 EFCONIVO).

References

[1] S. Barmada, L. Di Rienzo, N. Ida and S. Yuferev, "Time domain surface impedance concept for low frequency electromagnetic problemsPart I: Derivation of high order surface impedance boundary conditions in the time domain," IEE Proc.-Sci. Meas. Technol., vol. 152, no. 4, pp. 175–185, July 2005.

[2] S. Barmada, L. Di Rienzo, N. Ida and S. Yuferev, "The use of surface impedance boundary conditions in time domain problems: numerical and experimental validation," ACES Journal, vol. 19, no. 2, pp. 76–83, July 2004.

[3] L. Krähenbühl, O. Fabrègue, S. Wanser, M. De Sousa Dias and A. Nicolas, "Surface impedances, BIEM and FEM coupled with 1D non linear solutions to solve 3D high frequency eddy current problems," IEEE Trans. Magn., vol. 33, no. 2, pp. 1167–1172, March 1997.

[4] K.R. Davey and L. Turner, "Transient eddy current analysis for generalized structures using surface impedances and the fast Fourier transform," IEEE Trans. Magn., vol. 26, no. 3, pp. 1164–1170, May 1990.

[5] D. Rodger and H.C. Lai, "A surface impedance method for 3D time transient problems," IEEE Trans. Magn., vol. 35, no. 3, pp. 1369–1371, May 1999.

[6] J. Gyselinck, P. Dular, C. Geuzaine, R. V. Sabariego, "Surface-impedance boundary conditions in time-domain finite-element calculations using the magnetic-vector-potential formulation", IEEE Trans. Magn., vol. 45, no. 3, pp. 1280–1283, March 2009.

[7] J. Gyselinck, P. Dular, C. Geuzaine, and R. V. Sabariego, "Surface impedance boundary conditions for the modeling of saturable massive conducting volumes in time-domain finite-element calculations," in *Proceedings of 6ème Conférence Européenne sur les Méthodes Numériques en Electromagnétisme (NUMELEC2008)*, Liege, Belgium, December 8–10, 2008.

[8] A. Bossavit, "A rationale for edge-elements in 3-D fields computations," IEEE Trans. Magn., vol. 24, no. 1, pp. 74–79, July 1988.